Article

Tumor-Targeting Micelles Based on Linear-Dendritic PEG-PTX8 Conjugate for Triple Negative Breast Cancer Therapy

Yujie Zhang, Yifei Lu, Yu Zhang, Xi He, Qinjun Chen, Lisha Liu, Xinli Chen, Chunhui Ruan, Tao Sun, and Chen Jiang

Mol. Pharmaceutics, **Just Accepted Manuscript** • DOI: 10.1021/acs.molpharmaceut.7b00430 • Publication Date (Web): 23 Aug 2017

Tumor-Targeting Micelles Based on Linear-Dendritic PEG-PTX_8 Conjugate for Triple Negative Breast Cancer Therapy

Yujie Zhang, Yifei Lu, Yu Zhang, Xi he, Qinjun Chen, Lisha Liu, Xinli Chen, Chunhui Ruan, Tao Sun, Chen Jiang[*]

Key Laboratory of Smart Drug Delivery, Ministry of Education, State Key Laboratory of Medical Neurobiology, Department of Pharmaceutics, School of Pharmacy, Fudan University, Shanghai 200032, China

[*] Corresponding author: Chen Jiang, Tel: +86-21-5198-0079; Fax: +86-21-5198-0079; E-mail: jiangchen@shmu.edu.cn.

Table of Contents/Abstract Graphic

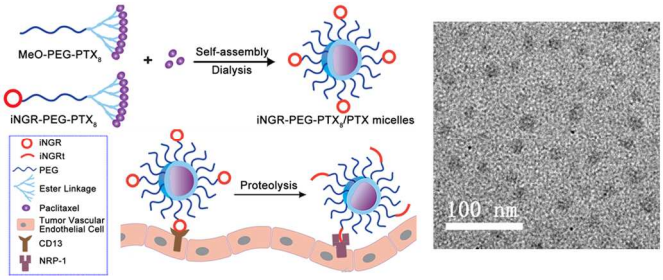

KEYWORDS: polymer-drug conjugates, linear-dendritic, micelle, triple negative breast cancer, tumor targeting

ABSTRACT: Most small molecular chemotherapeutics have poor water-solubility, unexpected pharmacokinetics and toxicity to normal tissues. A series of nano drug delivery systems have been developed to solve the problems, among which micelle based on linear-dendritic polymer-drug conjugates (LDPDCs) is a promising strategy to deliver hydrophobic chemotherapeutics due to its small size, fine stability in blood circulation and high drug loading capacity. In this work we synthesized a novel amphiphilic linear-dendritic PEG-PTX_8 conjugate which can also encapsulate extra free PTX and self-assemble into uniform ultra-small micelles with a hydrated diameter of 25.50±0.27 nm. To realize efficient drug delivery to tumor sites, a cyclic tumor homing and penetrating peptide iNGR was linked to the PEG-PTX_8 conjugate. The biological evaluation was performed on a human triple negative breast cancer model. PTX accumulation in tumor at 24 h of the TNBC-bearing mice treated with iNGR-PEG-PTX_8/PTX micelles was significantly enhanced ($P<0.001$, two-way ANOVA) compared to that of Taxol and untargeted MeO-PEG-PTX_8/PTX micelles. Furthermore, iNGR-PEG-PTX_8/PTX micelles showed obviously strong antitumor effect and the median survival time of TNBC bearing mice treated with iNGR-

modified micelles was significantly extended compared to Taxol. Therefore, this smart micelle system may be a favorable platform for effective TNBC therapy.

INTRODUCTION

Most small molecular anticancer drugs are poorly water-soluble, eliminated quickly *in vivo*, lacking in tumor-targeting ability and toxic to normal tissues. These disadvantages greatly limited their therapeutic effect and clinical application.[1, 2] With the development of nanotechnology, a variety of innovative nano drug delivery systems (NDDS) including nanoparticles, liposomes and micelles have been explored to increase solubility, improve pharmacokinetics, enhance tumor targeting, decrease systemic toxicity and eventually achieve optimal therapeutic benefits of hydrophobic drugs.[3-10]

Many liposomal, micellar or particulate nano formulations load hydrophobic drugs through physical entrapment *via* hydrophobic interaction. However, the resulting nanoparticles generally have low drug loading content and the weak intermolecular force may lead to internal instability of the nanoparticle structure and burst drug release in physiological medium.[11, 12] Even the FDA approved Abraxane, a nanoparticle formulation of albumin bounded paclitaxel (PTX), was found unstable in blood circulation, leading to drug leakage, unexpected pharmacokinetic properties, and off-target effect post-administration.[13, 14]

Another strategy for NDDS is to link the hydrophobic therapeutics to macromolecules or polymers through covalent bonds. The covalent linkage is more stable than the intermolecular force in blood circulation and premature drug release can be avoided.[15, 16] Micelle-forming polymer-drug conjugates (PDCs) is attracting increasing attention in the nanomedicine field due to its relatively good stability in blood stream and suitable assembled size (10-100 nm) to take advantage of EPR effect and accumulate in tumor site.[17-20] Over the past decades, researchers

have synthesized various PDCs with different architectures. Traditional linear PDCs usually linked mono drug molecule and the use of high molecular weight linear polymers often leads to low drug loading content.[7, 21] Additionally, drug conjugation might change the polymer composition or amphiphilicity, which could disrupt the nanostructure formation.[22] Graft-copolymer-drug conjugates can conjugate several drug molecules onto the side chains, but the grafted copolymer is composed of more than one organic monomers with appropriate polymerization degree, so the total molecular weight is always high, and the steric hindrance of the reactive side chains will increase difficulty for drug conjugation, resulting in reduced drug loading capacity.[23] Moreover, reagents used in the synthetic process of new polymeric materials might be toxic, non-biocompatible and remain in the materials, causing potential safety problems, and techniques employed in the nanostructure formation may have some limits.[24, 25] In comparison, linear-dendritic polymer-drug conjugate (LDPDC) is a unique class of PDC with well-defined structure, tunable aggregation properties, significantly increased drug loading content and superior stability.[22, 26-29] Therefore, it is a promising strategy to utilize LDPDC to delivery drugs for tumor therapy.

In this work, we aimed to design a novel LDPDC which utilize only one sort of dendritic polymer with favorable molecular weight to achieve improved drug properties such as longer blood circulation time, enhanced *in vivo* stability and targeting ability to tumor sites. PTX, a very potent chemotherapeutic agent and almost insoluble in water, was used as a model drug. Poly (ethylene glycol) (PEG) is one of the most widely used synthetic hydrophilic polymers with favorable biocompatibility and has been utilized to modify various hydrophobic chemotherapeutics to increase solubility and prolong blood circulation time.[30, 31] The commercial PEG-NH_2 (Mw=5000) was transformed into linear-dendritic PEG with eight hydroxyl ends

(PEG-OH_8) through three rounds of anhydride acylation and acid hydrolysis, then PTX was conjugated to PEG-OH_8 through a linker named 4-nitrophenyl chloroformate. With PEG as hydrophilic segment and PTX as the hydrophobic segment, the resulting LDPDC PEG-PTX_8 could self-assembly into stable homogeneous ultra-small micelles. Additionally, the amphiphilic dendritic PEG-PTX_8 can also serve as a drug carrier and encapsulate extra hydrophobic drugs into the hydrophobic core.

A promising drug delivery system should not only possess high drug loading capacity, good stability in blood stream but also realize targeted drug delivery into the lesion location. Since PTX is the first-line chemotherapeutics for the treatment of breast cancer, we intended to evaluate the linear-dendritic PEG-PTX_8 micelles on breast cancer. Triple negative breast cancer (TNBC) is the most malignant breast cancer subtype which lacks expression of estrogen receptor (ER), progesterone receptor (PR) and human epidermal growth factor receptor-2 (HER-2), accordingly it is considered relatively difficult to try targeted therapy for TNBC. It was reported that neuropilin-1 (NRP-1) is overexpressed on tumor vessels and TNBC, which can be considered as targets for drug delivery.[32-35] A novel designed cyclic peptide iNGR (CRNGRGPDC, C&C disulfide bridge) contains a vascular homing motif (NGR) and a CendR motif (R/KXXR/K) that can penetrate into tumor tissues more effectively than the standard NGR peptide.[36] In blood circulation, iNGR specifically and rapidly bound to CD13 overexpressed on the surfaces of tumor neovascular endothelial cells.[37] Afterwards, the cyclopeptide suffered a proteolytic process on the cell surface and exposed the internal CendR motif of iNGR. As a consequence, the resulting linear iNGRt (CRNGR) could penetrate tumor cells, which is mediated by NRP-1 (Scheme 1). This strategy allows the activation of the CendR motif only in the targeted tissue rich in neovasculature, avoiding NRP-1 activation in normal tissues.

Therefore, iNGR peptide was modified on the linear-dendritic PEG-PTX_8 conjugates to enhance targeting ability to TNBC. The *in vitro* and *in vivo* properties and effects of the iNGR-PEG-PTX_8 micelles were fully evaluated in the study.

Scheme 1. Schematic illustration presenting the preparation of iNGR-PEG-PTX8/PTX micelles and the *in vivo* performance through CD13 and NRP-1 receptors.

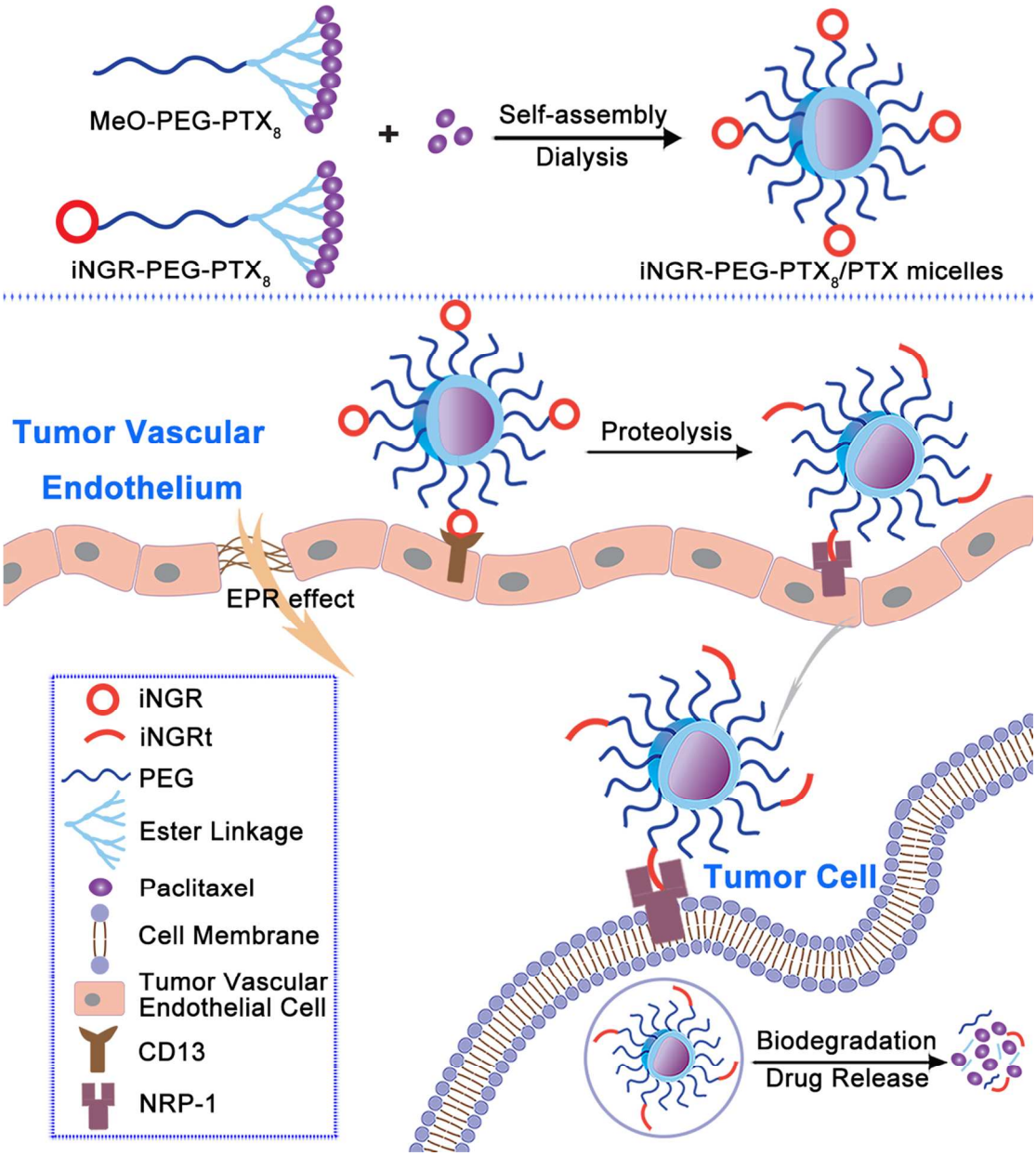

MATERIALS AND METHODS

Materials

Azide-PEG_{5k}-amine trifluoroacetic acid salt (N_3-PEG_{5k}-NH_2·TFA, Mw=5000) and Methoxy-PEG_{5k}-amine (MeO-PEG_{5k}-NH_2, Mw=5000) were purchased from Jenkem technology Co., Ltd. (Beijing, China). Paclitaxel (PTX) was purchased from Meilune Biological technology Co., Ltd. (Dalian, China). iNGR and iNGRt peptides with alkynyl modification were synthesized by China Peptides Co., Ltd. (Suzhou, China). Sodium ascorbate, 4-dimethylaminopyridine (DMAP) and N,N,N′,N″,N″-pentamethyldiethylenetriamine (PMDETA) were purchased from J&K chemical Co., Ltd. (Shanghai, China). [4,5-dimethylthiazol-2-yl]-2,5-diphenyl tetrazolium bromide (MTT) and coumarin-6 were purchased from Sigma-Aldrich (St. Louis, MO, USA). Benzaldehyde dimethyl acetal, 2,2-Bis (hydroxymethyl) propionic acid, tert-butyl methyl ether (TBME) and 4-(2-hydroxyethyl)-1-piperazineethanesulfonic acid (HEPES) was purchased from Aladdin Industrial Corporation (Shanghai, China). Fluorescent dye BODIPY was synthesized according to the literature before. All other chemicals were purchased from Sinopharm Chemical Reagent Co., Ltd (Shanghai, China) unless mentioned otherwise.

Eagle's Medium (DMEM) and fetal bovine serum (FBS) were purchased from Gibco BRL (Carlsbad, CA, USA). DNA Fragmentation Detection Kit and Cell Cycle Detection Kit were purchased from KeyGEN BioTECH (Nanjing, China). ^{33}D-luciferin potassium was purchased from Pierce (Rockford, USA).

Human umbilical vein endothelial cells (HUVECs) was obtained from American Type Culture Collection (ATCC, Rockville, MD, USA). MDA-MB-231 cell line was purchased from Shanghai institutes for cell resource center, Chinese Academy of Sciences (Shanghai, China). MDA-MB-231/luci cell line was purchased from Cell Biolabs, Inc (San Diego, USA). Female

SD rats and nude mice were supplied by the Animal Center of School of Pharmacy, Fudan University.

Synthesize and characterization of linear-dendritic PEG-PTX_8 Conjugates.

MeO-PEG-OH_8 and N_3-PEG-OH_8 were synthesized according to the synthetic route (Figure 1) as described previously.[27] MeO-PEG-OH_2 and MeO-PEG-OH_4 were also produced during the process. PTX was conjugated to MeO-PEG-OH_n (n=2, 4, 8) and N_3-PEG-OH_8 using 4-nitrophenyl chloroformate as a linker. In brief, benzylidene-2, 2-bis(oxymethyl) propionic anhydride (BBOPA) was synthesized through two steps of dehydration-condensation reaction. Then MeO-PEG-NH_2 (Mw=5000) and N_3-PEG-NH_2 (Mw=5000) were transformed into MeO-PEG-OH_8 and N_3-PEG-OH_8 respectively through three rounds of BBOPA acylation and acid hydrolysis. MeO-PEG-OH_8 (150 mg, 1 equiv.) and excess 4-nitrophenyl chloroformate (387 mg, 64 equiv.) were dissolved in 5 mL dry dichloromethane (DCM) under the protection of nitrogen, then pyridine (309 μL, 128 equiv.) was added dropwise. The reaction mixture was stirred at room temperature for 24 h. After completion, the white precipitation was filtered off and washed with cold DCM. Then the filtrate was concentrated and purified by column chromatography on Sephadex LH 20 using methanol as eluent. The solvent was removed under reduced pressure to get the desired product (a7 in Figure 1). Then PTX (20 equiv.) and DMAP (4 equiv.) were added to the above product and dissolved in 4 mL of dry DCM under the protection of nitrogen. After 24 h stirring under room temperature, the mixture was also purified on Sephadex LH 20 to get the target product MeO-PEG-PTX_8. N_3-PEG-PTX_8 was synthesized by the same procedures. Finally 237 mg MeO-PEG-PTX_8 and 307.5 mg N_3-PEG-PTX_8 was obtained. By the way, MeO-PEG-PTX_2 and MeO-PEG-PTX_4 were also synthesized and purified in the same method.

Alkynyl iNGR (or iNGRt) peptide was linked to the terminus of N_3-PEG-PTX_8 *via* copper(I)-catalyzed azide-alkyne cycloaddition (CuAAC) click reaction. N_3-PEG_{5k}-PTX_8 (85 mg, 1 equiv.) and excess alkynylated iNGR (27 mg, 3 equiv.) were dissolved in 3 mL of dry dimethylformamide, then sodium ascorbate (15 mg, 9 equiv.), PMDETA (5.4 μL, 3 equiv.) and solid CuI (4.8 mg, 3 equiv.) were added to the solution in order. The whole process was carried out under the protection of Argon. The reactant was stirred for 12 h at 40 □. After completion, The mixture was dialyzed against PBS buffer containing 10 mM EDTA-2Na (pH=7.4) for 12 h, deionized water for 24 h, followed by freeze-drying. Finally, 90 mg iNGR-PEG-PTX_8 and 30 mg iNGRt-PEG-PTX_8 were obtained.

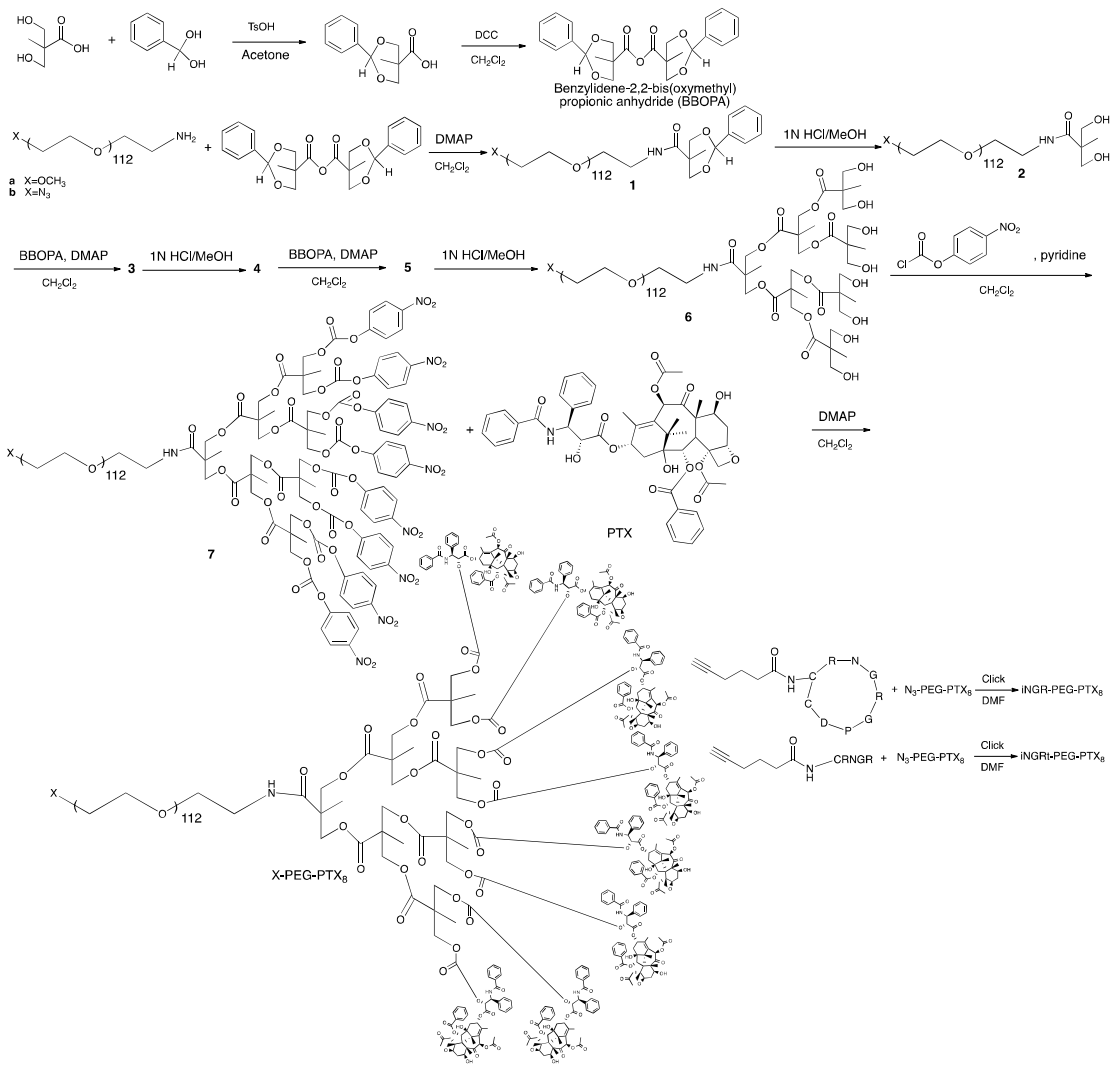

Figure 1. Synthetic route of MeO-PEG-PTX$_8$, iNGR-PEG-PTX$_8$ and iNGRt-PEG-PTX$_8$.

Products of each step were characterized by NMR spectrometer (400 MHz, Bruker, Billerica, MA), and iNGR-PEG-PTX$_8$ and iNGRt-PEG-PTX$_8$ were characterized by IR spectrum additionally.

Preparation and characterization of micelles based on different PEG-PTX conjugates.

To optimize the micelle formulation, a series of micelles composed of different linear-dendritic PEG-PTX conjugates and encapsulated PTX amount were prepared *via* dialysis method. In detail, a certain amount of PTX was weighed and dissolved in methanol to concentration of 1

mg/mL and all of the PEG-PTX conjugates were dissolved in methanol to final concentration of 5 mg/mL separately. 2 mg of each kind of PEG-PTX conjugates and 5%, 10%, 20% and 40% （w/w）free PTX were mixed up and vortex for 30 s and then sealed in a dialysis bag (diameter=18 mm, MWCO=5000) followed by dialysis against deionized water for 12 h. Then the liquid in dialysis bag was collected and filtered through a 0.22 μm filter to get the final micelle solution. Size and PDI of the freshly prepared micelles were measured by dynamic light scattering (DLS) (Zetasizer Nano-ZS, Malvern, U.K.) and re-measured at day 7. The morphological images of the PTX loaded micelles were photographed by transmission electron microscope (TEM, Tecnai G2 spirit Biotwin, FEI).

PTX loading capacity of the micelles was determined by HPLC through alkaline lysis method. Briefly, 10 μL of the micelles was diluted 10 times with distilled water and then treated with 100 μL of 2 N NaOH aqueous solution for 30 min at 37 °C water bath, afterwards, 200 μL of 1 N HCl aqueous solution was added to neutralize the excess alkaline. The salt produced in this step was precipitated by mixing with acetonitrile (ACN) and centrifuged at 12000 rpm for 10 min for three times. PTX standard sample was also treated with the same method to obtain the standard curve. 20 μL of the supernatant was analyzed by HPLC at 227 nm with 40% ACN and 60% H_2O as mobile phase.

***In vitro* PTX release studies.**

In vitro PTX release from the micelles was performed using dialysis method (n=3). In brief, 0.3 mL solution of free PTX (dissolved in methanol), Taxol, MeO-PEG-PTX_8/PTX and iNGR-PEG-PTX_8/PTX micelles with an equal PTX concentration (0.5 mg/mL) was sealed into a dialysis bag (MWCO=3500) and immediately placed into 12 mL dialysis medium (pH=7.4 PBS, containing 1N sodium salicylate). The experiment was carried out at 100 rpm, 37 °C on the

Shaking Bath for 72 h. 0.3 mL of the medium was withdrawn and equal volume of fresh release medium was replenished at various time points. PTX concentration of each sample was determined by HPLC at 227 nm.

Cell culture

MDA-MB-231 cells and MDA-MB-231/luci cells were grown in DMEM containing 10 mM HEPES and 10% FBS at 37 °C with 5% CO_2. HUVEC cells were cultured in DMEM added with 10% FBS and 1% v/v penicillin-streptomycin solution at 37 °C with 5% CO_2.

Cell uptake studies.

MDA-MB-231 cells and HUVECs were seeded in 24-well plates (Corning-Coaster, Tokyo, Japan) at a density of 8×10^4 cells per well. When achieving 80-90% confluence, the cells were incubated with non-targeting micelles (MeO-PEG-PTX_8 micelles), iNGR-modified micelles (with 10%, 20% and 40% iNGR modification) and iNGRt-modified micelles (with 20% iNGRt modification, determined by the cellular uptake results of iNGR-modified micelles) at the concentration of 20 μg/mL PEG-PTX_8 conjugates in serum-free DMEM. All the micelles were encapsulating with 0.5% (w/w) coumarin-6 as a fluorescent probe through dialysis method as described above. After 30 min incubation, cells were rinsed with PBS for three times and then 0.3 mL of Hank's was added to each well. The cellular uptake of micelles was visualized and photographed by inverted fluorescent microscope (Leica Wetzlar).

***In vitro* anticancer efficacy study.**

In vitro anticancer efficacy of the micelles was evaluated by MTT assay (n=4). MDA-MB-231 cells were seeded at a density of 5×10^3 cells/well in 96-well plates. After 24 h incubation, cells were then washed for three times with PBS and exposed to 200 μL of various concentrations of Taxol, MeO−PEG−PTX_8/PTX, 20% iNGR−PEG−PTX_8/PTX micelles (mentioned as iNGR-

PEG-PTX/PTX below) and 20% iNGRt−PEG−PTX_8 /PTX micelles (mentioned as iNGRt-PEG-PTX/PTX below) at 37 °C for 48 h. Then the medium was removed and cells were washed with PBS for three times and 150 μL of MTT (0.5 mg/mL) solution was added into each well and further incubated at 37 °C for 4 h. Next, the solution was sucked up and 200 μL of DMSO was added to each well to dissolve the formazan crystals formed by the living cells. Then the 96-well plates were balanced on the air bath for 10 min at 37 °C in the dark. Cells without treatment served as control. Absorbance was read at 570 nm by dual wavelength detection using a Multiskan MK3 microplate reader (Thermo Scientific, Waltham, Massachusetts, USA). Cell viability was calculated as the survival percentage of control.

Cell cycle analysis

MDA-MB-231 cells were seeded on a six-well plate and cultured at 37 °C for 24 h. When 80-90% confluence was reached, cells in each well were treated with different formulations of PTX at an equal concentration of PTX (1 μg/mL) in FBS-free medium. After a 30-min incubation, the medium was removed and cells were washed with Hank's for three times and cultured with fresh complete medium for another 24 h. Next, Cells were collected and centrifuged at 2000 rpm, then washed with cold PBS and fixed with 500 μL cold 70% ethanol overnight. Then the fixed cell suspension was centrifuged and washed with PBS redispersed in 300 μL PBS. Cells were treated with RNase A for 30 min at 37 °C and then with 80 μL PI for another 30 min. Fluorescence was measured by a flow cytometer (FACS, BD Biosciences, Bedford, MA) and histograms of cell number versus PI intensity were used to determine the percentage of cells in each phase of the cell cycle.

Modeling of triple negative breast cancer.

Female BALB/C nude mice of ~20 g body weight were xenografted with 1×10^6 MDA-MB-231/luci cells which were suspended in 100 μL Matrigel solution (5 mg/mL in PBS) by *in situ* injection into the second right mammary fat pad of nude mice and were raised under SPF laboratory conditions.

***In vivo* imaging.**

Aza-BODIPY (Ex=700 nm, Em=730 nm) was encapsulated as a NIR probe in the non-targeting and iNGR-modified micelles at a final concentration of 20 μg/mL. Micelles were injected intravenously *via* tail vein into MDA-MB-231 bearing mice at concentration of 0.2 mg BODIPY/kg. The *in vivo* biodistrabution of micelles at different time was traced and visualized by Xenogen IVIS Spectrum with Living Image Software 4.2 (Caliper Life Science, Hopkinton, Massachusetts, USA). Mice were sacrificed at 24 h and tumors and organs was collected *ex vivo* and also photographed by IVIS.

Pharmacokinetics and Biodistribution studies.

To investigate *in vivo* pharmacokinetics (PK) of the MeO-PEG-PTX_8/PTX and iNGR-PEG-PTX_8/PTX micelles, healthy female SD rats were fasting for 18 h before experiment. The rats were randomly divided into three groups and then administrated with Taxol, MeO-PEG-PTX_8 /PTX and iNGR-PEG-PTX_8/PTX micelles at a dose of 10 mg PTX/kg *via* caudal vein injection (n=6) respectively. 0.5 mL blood was collected at each time point and centrifuged at 3500 rpm for 10 min to get supernatant for further treatment. Diazepam was used as an internal standard for determination of PTX concentration. All the plasma samples were treated by the previous method and analyzed by HPLC.

Biodistribution of PTX in MDA-MB-231 bearing nude mice was performed when tumor volume reached approximately 500 mm^3 (n=4). Taxol and the micelles were also injected *via* tail

vein at the same dose of PK test. Mice were sacrificed at 2 h and 24 h separately. Tumors and normal organs (including heart, liver, spleen, lung and kidney) were taken out, washed with cold saline, dried over filter paper, weighed and stored at -20 °C before analysis. Docetaxel (DTX) was employed as an internal standard. The samples was prepared as described[38] and PTX concentration was measured by LC/MS/MS (AB 4000 Q TRAP). ZORBAX 300 Extend-C18 column (2.1×150 mm, 3.5 μm) was employed and flow rate was 0.2 mL/min. the mobile phase was 80% methanol and 20% water containing 0.1% formic acid. The retention time of PTX and DTX was 2.18 min and 2.26 min separately.

Antitumor efficacy

Nude mice with MDA-MB-231/luci xenograft were randomly divided into four groups (n=6) according to the bioluminescence signal scanned by the *in vivo* real-time bioluminescence system which reflects the tumor size of the mice. The mice were administrated with saline, Taxol, MeO−PEG_{5k}−PTX_8/PTX and iNGR−PEG_{5k}−PTX_8/PTX micelles (at an equal dose of 10 mg/kg PTX) at day 15 post implantation. Weight and tumor volume were measured every other day.

Terminal deoxynucleotidyl transferase dUTP nick-end labeling (TUNEL) assay was performed on frozen tumor slices from TNBC bearing mice administrated with different PTX formulations using a DNA fragmentation detection kit according to the instruction. Pictures of the stained tumor slices were photographed under the inverted fluorescent microscope.

RESULTS AND DISCUSSION

Synthesize and characterization of linear-dendritic PEG-PTX_8 Conjugates

Compound BBOPA, polymer a1-a7, b1-b7, MeO-PEG-PTX_2 and MeO-PEG-PTX_4 were all successfully synthesized and characterized by ^{1}H NMR spectra (Supporting Information, Figure

S1-S18). As shown in Figure 2A and 2B, peaks between 7 and 8 ppm represent the protons of aryl ring of PTX and peaks at 3.5-3.6 ppm represent the protons of repeated ethylene oxide unit of PEG, which indicate the successful synthesis of MeO-PEG-PTX_8 and N_3-PEG-PTX_8. Calculated by ^1H NMR spectrum, 6.67 and 6.56 PTX was conjugated to MeO-PEG-OH_8 and N_3-PEG-OH_8 per molecule on average, respectively. iNGR-PEG-PTX_8 and iNGRt-PEG-PTX8 were characterized by IR spectra additionally. The azide peak of N_3-PEG-PTX_8 showed on IR spectrum was ~2109 cm^{-1}, and the peak was disappeared on the IR spectrum of iNGR-PEG-PTX_8 (Figure 2C) and iNGRt-PEG-PTX_8 (Figure 2D), suggesting that the desired conjugates were synthesized successfully.

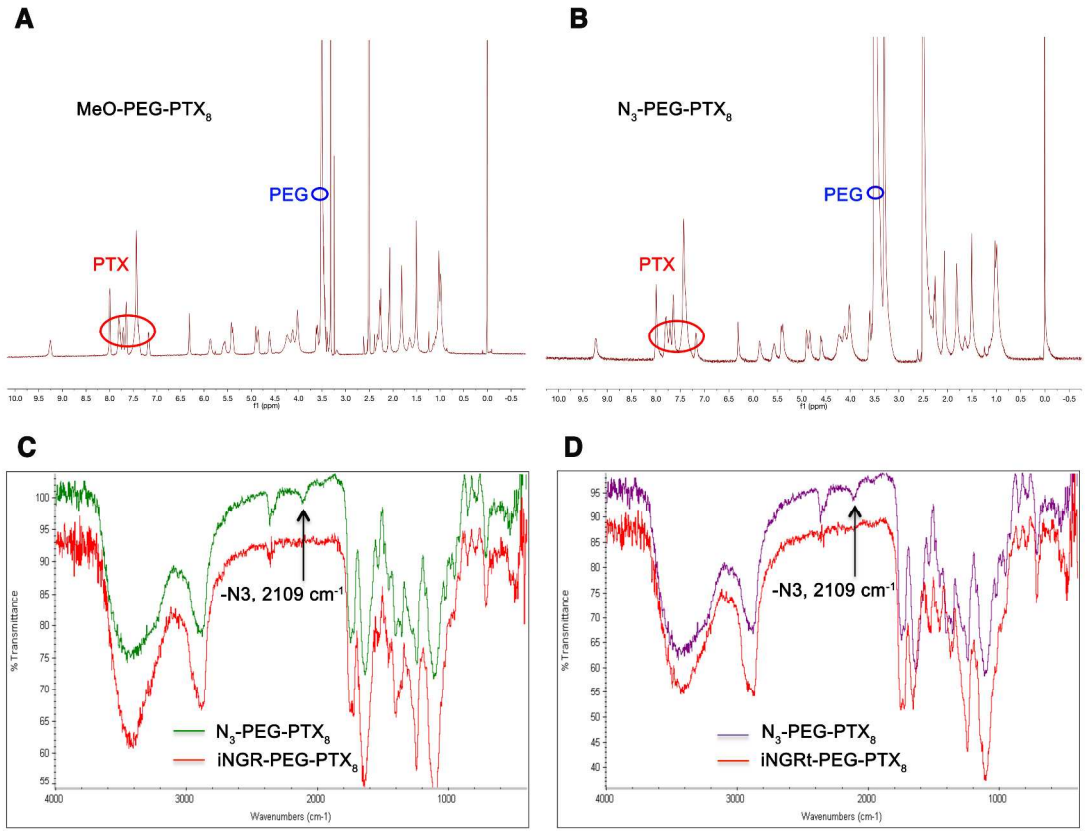

Figure 2. Characterization of different PEG-PTX_8 conjugates. (A) ^1H NMR spectrum of MeO-PEG-PTX_8; (B) ^1H NMR spectrum of N_3-PEG-PTX_8; (C) IR spectrum of iNGR-PEG-PTX_8 and (D) IR spectrum of iNGRt-PEG-PTX_8.

Preparation and characterization of micelles based on different PEG-PTX conjugates.

Since the linear-dendritic PEG-PTX_n (n=2, 4, 8) conjugates are amphiphilic, we assumed that they could also serve as carriers to load free hydrophobic drugs in the hydrophobic core. Therefore, we prepared a series of micelles with different amount of free PTX to get the optimal formulation of the PEG-PTX based micelles. Size distribution and PDI of micelles based on different PEG-PTX conjugates was concluded in Figure 3A and 3B, separately. We found that micelle structures formed spontaneously upon dialysis against deionized H_2O. By comparison in size, PDI and dynamic stability, the micelle of PEG-PTX_8 encapsulated 5% free PTX was considered as the optimal formulation with good fine *in vitro* stability, low PDI and ultra-small size (Table 1). When incubated with 10% FBS at 37 □ for 12 h or diluted 10 and 100 times with PBS (pH=7.4) buffer, the micelles size showed no significant change (Supporting Information, Figure S19 and Figure S20), which proved that it was considerably stable against serum and dilution in physiological buffers.

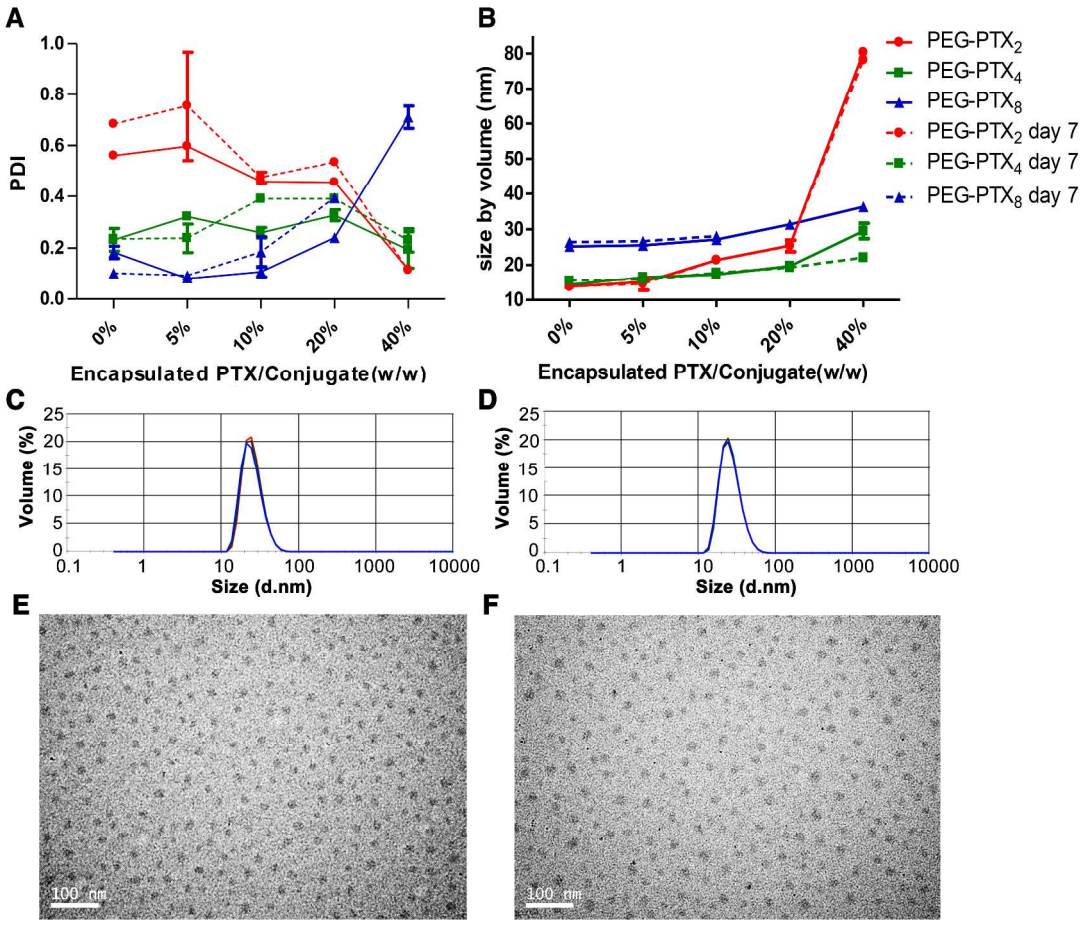

Figure 3. Characterization of various micelles. (A) PDI and (B) size distribution of different micelles based on PEG-PTX conjugates (n=3); Size distribution by DLS of (C) MeO-PEG-PTX8/PTX micelles and (D) iNGR-PEG-PTX8/PTX micelles (n=3); and representative TEM images of (E) MeO-PEG-PTX8/PTX micelles and (F) iNGR-PEG-PTX8/PTX micelles.

TEM images show that the morphology of MeO-PEG-PTX_8/PTX and iNGR-PEG-PTX_8/PTX micelles is core-shelled and homogeneous (Figure 3E and 3F) with diameter of 19.81 ± 0.47 nm and 21.47 ± 0.47 nm respectively, which are slightly smaller than the hydrated diameters measured by DLS.

Through HPLC determination, drug loading capacity of MeO-PEG-PTX_8/PTX and iNGR-PEG-PTX_8/PTX micelles was 54.70 ± 1.41% and 52.26 ± 0.77%, respectively, higher than most

PTX-loaded nanoparticles and micelles reported before. The overall properties of the PTX loaded micelles were summarized in Table 1.

Table 1. Summary of micelle properties (Data are presented as mean ± SD, n=3).

Formulation	Size (Z-Average, d.nm)	PDI	Drug Loading Capacity (%)
MeO-PEG-PTX_8/PTX	25.50 ± 0.27	0.082 ± 0.002	54.70 ± 1.41
iNGR-PEG-PTX_8/PTX	26.17 ± 0.13	0.126 ± 0.014	52.26 ± 0.77
iNGRt-PEG-PTX_8/PTX	29.06 ± 0.31	0.142 ± 0.022	53.17 ± 0.62

***In vitro* PTX release studies.**

The *in vitro* drug release properties under physiological condition was simulated by dialysis method in PBS (pH=7.4). As shown in Figure 4, free PTX was rapidly released from the dialysis bag (MWCO=3500) while PTX release rate from Taxol was relatively slow. This is because the solvent of Taxol, Cremophor EL, is an amphiphilic polymer as well as a surfactant which can form micelles and encapsulate PTX in the core by self-assembling upon countering with water. Both of the MeO-PEG-PTX_8/PTX and iNGR-PEG-PTX_8/PTX micelles only release ~10% of total PTX until 72 h, which indicated that the covalent linkage between PEG and PTX were relatively stable under physiological conditions and burst release of the loaded drug was avoided to some extent. However, the sufficient enzymes in the tumor cells permit an accelerated hydrolysis of the carbonate ester to release PTX.[39, 40] The drug biodistribution study (see below) also proved that prototype PTX was released from the micelles in the tissues.

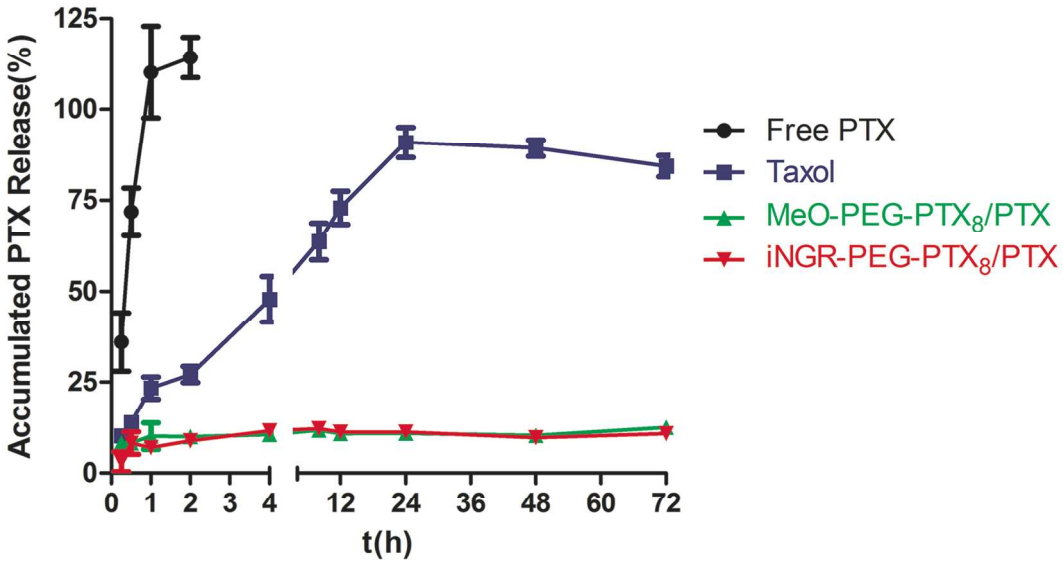

Figure 4. *In vitro* drug release behaviors from different PTX formulations in PBS (pH 7.4) at 37 °C with free PTX (dissolved in methanol) as the control group. Data are represented as mean ± SD (n = 3).

Cellular uptake of the micelles.

HUVEC is widely used as a model to mimic tumor neovascular cells and it was reported that CD13, NRP-1/2, and Matriptase are overexpressed on HUVECs.[30-35] Human MDA-MB-231 cell line overexpresses NRP-1 and was chosen to mimic TNBC. The cellular uptake efficiency of the micelles was evaluated in HUVECs and MDA-MB-231 cells. Firstly micelles with different percent of iNGR-PEG-PTX_8 (w/w) at a concentration of 20 μg/mL PEG-PTX_8 conjugates were co-incubated with HUVECs and 20% iNGR-PEG-PTX_8/PTX micelles showed enough targeting to HUVECs (Supporting Information, Figure S21). So we selected 20% iNGR-modified micelles and 20% iNGRt-modified micelles to do subsequent experiments. Images under fluorescence microscope suggested that HUVECs treated with iNGR-PEG-PTX_8/Cou6 and iNGRt-PEG-PTX_8/Cou6 micelles exhibited obviously enhanced internalization compared to non-targeting

MeO-PEG-PTX_8/Cou6 micelles (Figure 5). MDA-MB-231 cells treated with iNGRt-PEG-PTX_8/Cou6 showed significantly higher uptake efficiency than non-modified micelles because iNGRt-modified micelles can be internalized through NRP-1 mediated process (Figure 6). In addition, MDA-MB-231 cells treated with iNGR-PEG-PTX_8/Cou6 micelles showed slightly higher fluorescence because it is negative on CD13 expression, while it expresses matriptase at a low level which can cleave cyclic iNGR peptide into linear iNGRt peptide, and realize active targeting through NRP-1 pathway. The cellular uptake study was also performed on a CD13- and NRP-1-negative cell line HEK293 and there was no significant difference in fluorescence of HEK293 cells treated with the non-targeting, iNGR-modified and iNGRt-modified micelles (as shown in Figure S23).

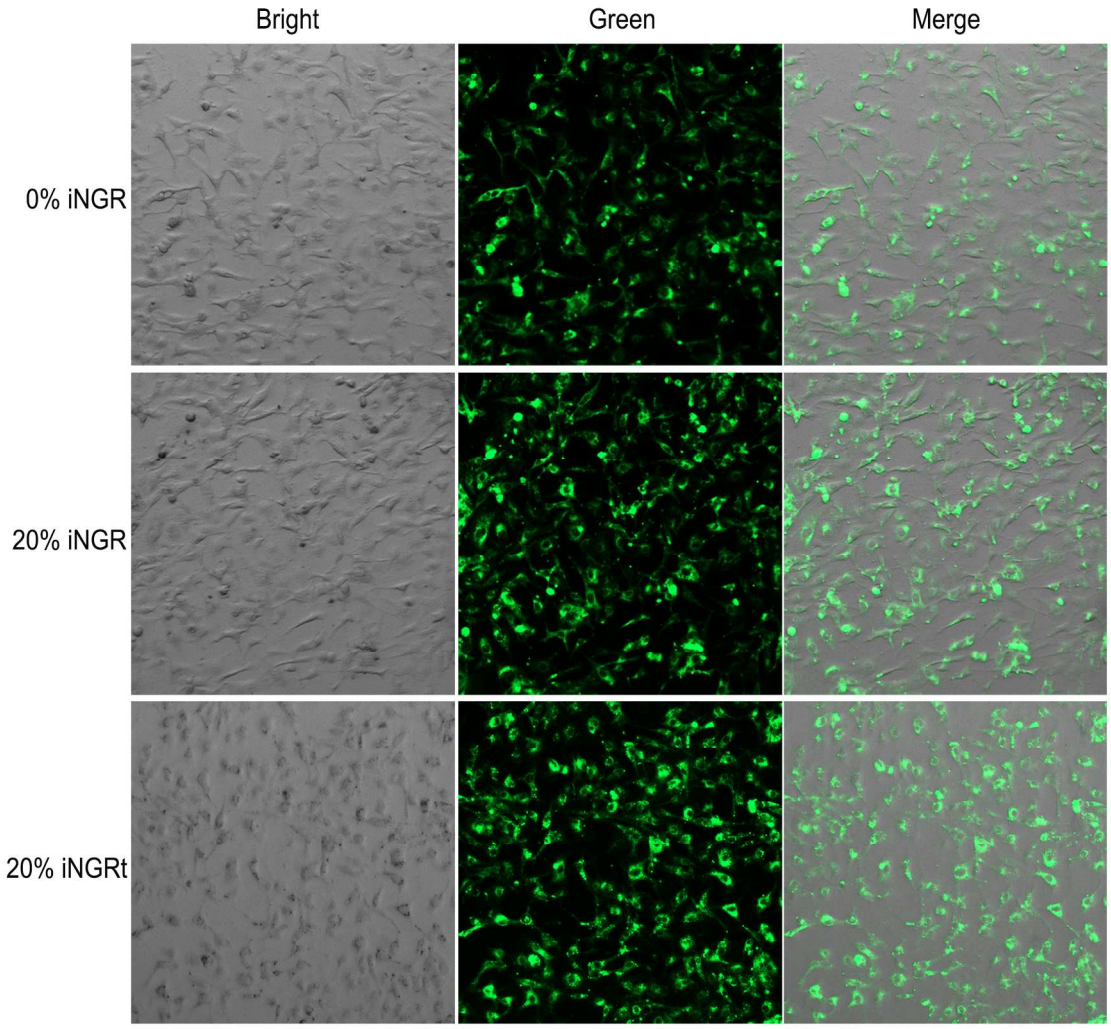

Figure 5. Cellular uptake of coumarin-6 loaded PEG-PTX8 micelles with different modification on HUVEC cells (original magnification: 50×). Green: fluorescence signal of coumarin-6.

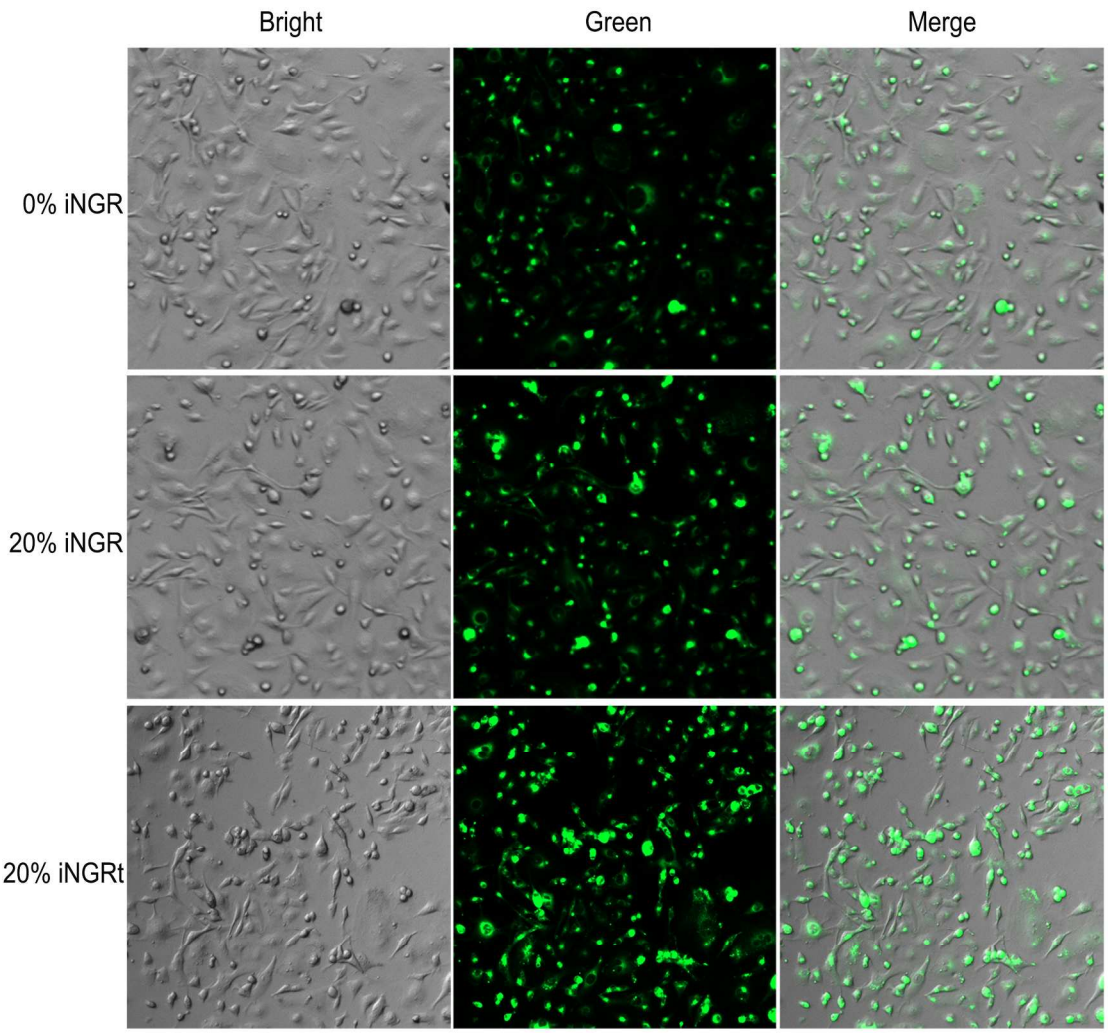

Figure 6. Cellular uptake of coumarin-6 loaded PEG-PTX8 micelles with different modification on MDA-MB-231 cells (original magnification: 50×). Green: fluorescence signal of coumarin-6.

***In vitro* anticancer efficacy.**

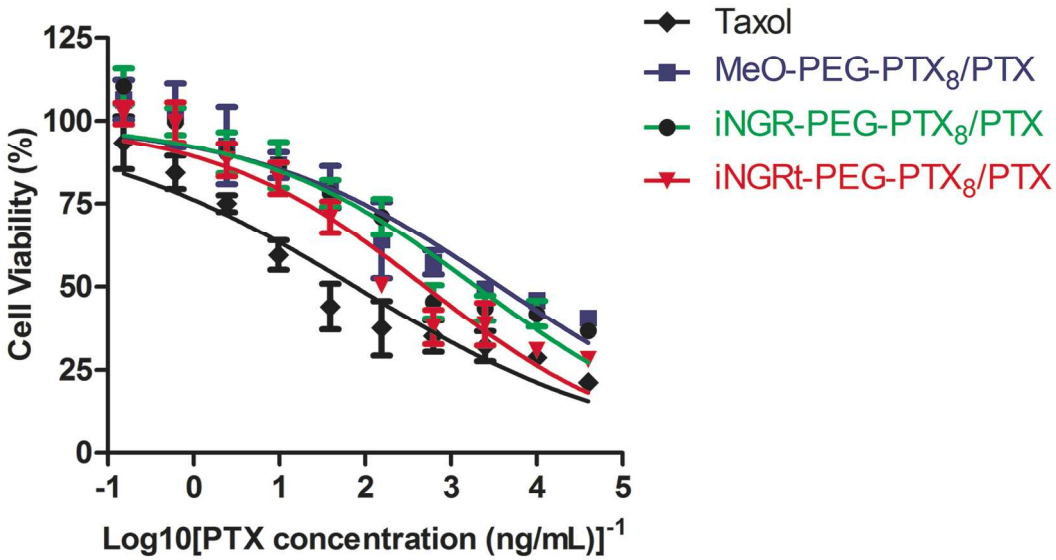

Figure 7. *In vitro* cytotoxicity of different PTX formulations at various concentrations against MDA-MB-231 tumor cells 48 h after incubation. Data are represented as mean ± SD (n = 4).

Table 2. IC_{50} values of different PTX formulations against MDA-MB-231 tumor cells (Data are presented as mean ± SD, n = 4).

Formulation	Taxol	MeO-PEG-PTX_8/PTX	iNGR-PEG-PTX_8/PTX	iNGRt-PEG-PTX_8/PTX
IC_{50} (ng/mL)	76.69 ± 1.27	3774 ± 1.33	1991 ± 1.29	503.6 ± 1.23

In vitro cytotoxicity of Taxol, MeO-PEG_{5k}-PTX_8/PTX, iNGR-PEG_{5k}-PTX_8/PTX and iNGRt-PEG_{5k}-PTX_8/PTX micelles against MDA-MB-231 cells were investigated by MTT assay. Figure 7 displayed that different PTX formulations inhibited cell viability at a dose-dependent manner. It was shown that the IC_{50} of iNGRt-PEG-PTX_8/PTX micelles (503.6 □□1.23 ng/mL) was significantly lower than iNGR-PEG-PTX_8/PTX micelles (1991 □□1.29 ng/mL) and MeO-PEG-PTX_8/PTX micelles (3774 □□1.33 ng/mL). Cytotoxicity is dependent on the intracellular drug concentration, so the results are consistent with the cellular uptake results. Interestingly, all of

the micelles have higher IC_{50} value than that of Taxol (76.69□1.27 ng/mL) (Table 2), which is possibly because Cremophor EL is also attributed to cytotoxicity[41-43] and PTX was not fully released from the micelles. Actually, we have investigated the stability of the micelles in cell culture medium (DMEM+10% FBS+1% Penecillin-Streptomycin solution) with MDA-MB-231 cells (detailed method was in supporting information), Different micelles were co-incubated with MDA-MB-231 cells at an equal PTX concentration (2.5 μg/mL PTX). Results showed that at 1 h, less than 1% of MeO-PEG-PTX_8 was released while ~7% of MeO-PEG-PTX_8/PTX released in cell culture medium with tumor cells, which suggested that the micelles were disintegrated inside the cells and the physically encapsulated free PTX (5%, w/w) was fully released within 1 h while little conjugated PTX was released (as shown in **Figure S24** in supporting information). The accumulated PTX release of the micelles was not significantly increased until 24 h and the iNGR-modified micelles showed similar release property, indicating that the carbonate ester bond remains relatively stable in the medium with MDA-MB-231 cells. As the *in vitro* cytotoxicity results (**Figure 7**) displayed that tumor cells were induced to apoptosis by the MeO-PEG-PTX_8/PTX and iNGR-PEG-PTX_8/PTX micelles in a concentration-dependent manner, and **Figure 12** (see below in the "Antitumor efficacy" section) demonstrated that the micelles have stronger *in vivo* anti-tumor effect, it could be indirectly concluded that the conjugated PTX could also induce cell apoptosis in a similar way as free PTX.

Cell cycle distribution.

PTX is well known to suppress cell proliferation by inhibiting microtubule disassembly and arrest cell cycle in the G2/M phase. To investigate the mechanism by which the PEG-PTX_8/PTX micelles inhibit cell proliferation, the population of MDA-MB-231 cells in different cell cycle stages was quantified by FACS analysis of ~10000 cells per sample. Figure 8 concluded the

results of cell cycle distribution after co-incubation with Taxol, MeO-PEG-PTX_8/PTX, iNGR-PEG-PTX_8/PTX and iNGRt-PEG-PTX_8/PTX micelles at a concentration of 1 μg/mL PTX equivalent respectively. Compared to untreated MDA-MB-231 cells (control, 13.75% G2/M phase), Taxol caused a markedly increased accumulation of G2/M phase cells (46.00%)，while the percentage of cells treated with MeO-PEG-PTX_8/PTX micelles, iNGR-PEG-PTX_8/PTX micelles and iNGRt-PEG-PTX_8/PTX micelles in G2/M phase was 32.18%, 30.62% and 39.86%, respectively. iNGRt-PEG-PTX_8/PTX micelles induced the strongest cell arrest effect among the groups because cellular uptake efficiency was enhanced by NRP-1 mediating pathway in accordance with the cellular uptake results. The percentages of cell population in each phase of the cell cycle are summarized in Table 3.

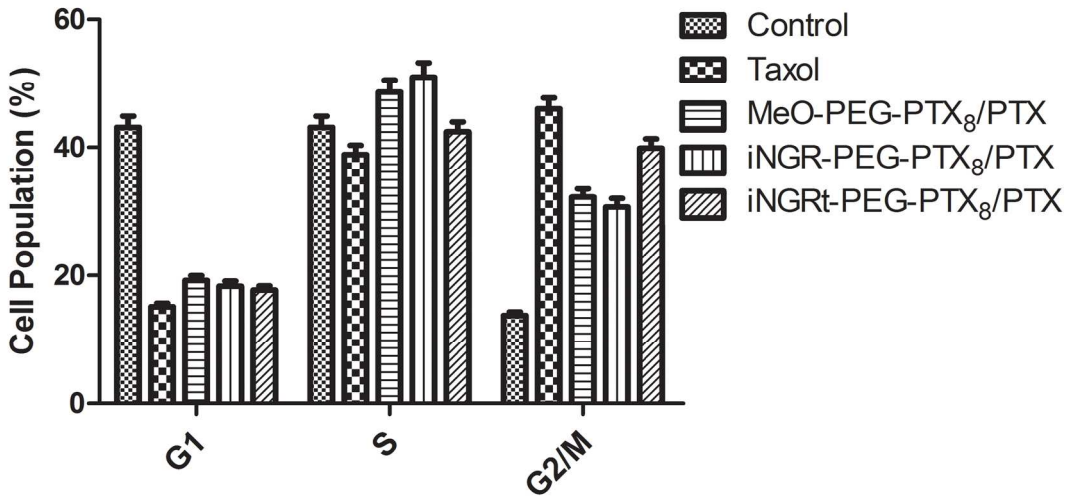

Figure 8. Cell cycle analysis of MDA-MB-231 cells treated with different PTX formulation at a concentration of 1 μg/mL PTX.

Table 3. Cell population in each phase of MDA-MB-231 cells treated with different PTX formulations.

Cell population (%)	G1 Phase	S Phase	G2/M Phase

Control	43.12	43.13	13.75
Taxol	15.11	38.89	46.00
MeO-PEG-PTX_8/PTX	19.20	48.63	32.18
iNGR-PEG-PTX_8/PTX	18.34	51.04	30.62
iNGRt-PEG-PTX_8/PTX	17.71	42.43	39.86

***In vivo* imaging.**

In vivo imaging was employed to evaluate the targeting efficiency of BODIPY loaded iNGR-PEG-PTX_8 micelle and MeO-PEG-PTX_8 micelle in TNBC-bearing nude mice. As displayed in Figure 9 A, mice treated with iNGR-PEG-PTX_8/PTX micelles exhibited stronger near-infrared（NIR）signal at 24 h after intravenously injection through tail vein comparing with MeO-PEG-PTX_8/PTX micelles at the tumor site, showing enhanced tumor targeting ability with iNGR peptide modification. 3D image of the tumor site was captured at the same time (Figure 9B). Moreover, tumors and the major organs were excised for *ex vivo* imaging to observe the tissue distribution (Figure 9C). Tumor of TNBC-bearing mice treated with iNGR-PEG-PTX_8/PTX micelles also showed stronger signal than that of MeO-PEG-PTX_8/PTX micelles. Furthermore, NIR fluorescence intensity in normal tissues was much weaker than that in tumors for both groups, which suggested that besides active targeting, the micelles took good advantage of EPR effect due to its ultra-small size and high stability in blood circulation, resulting in reduced toxicity to normal tissues.

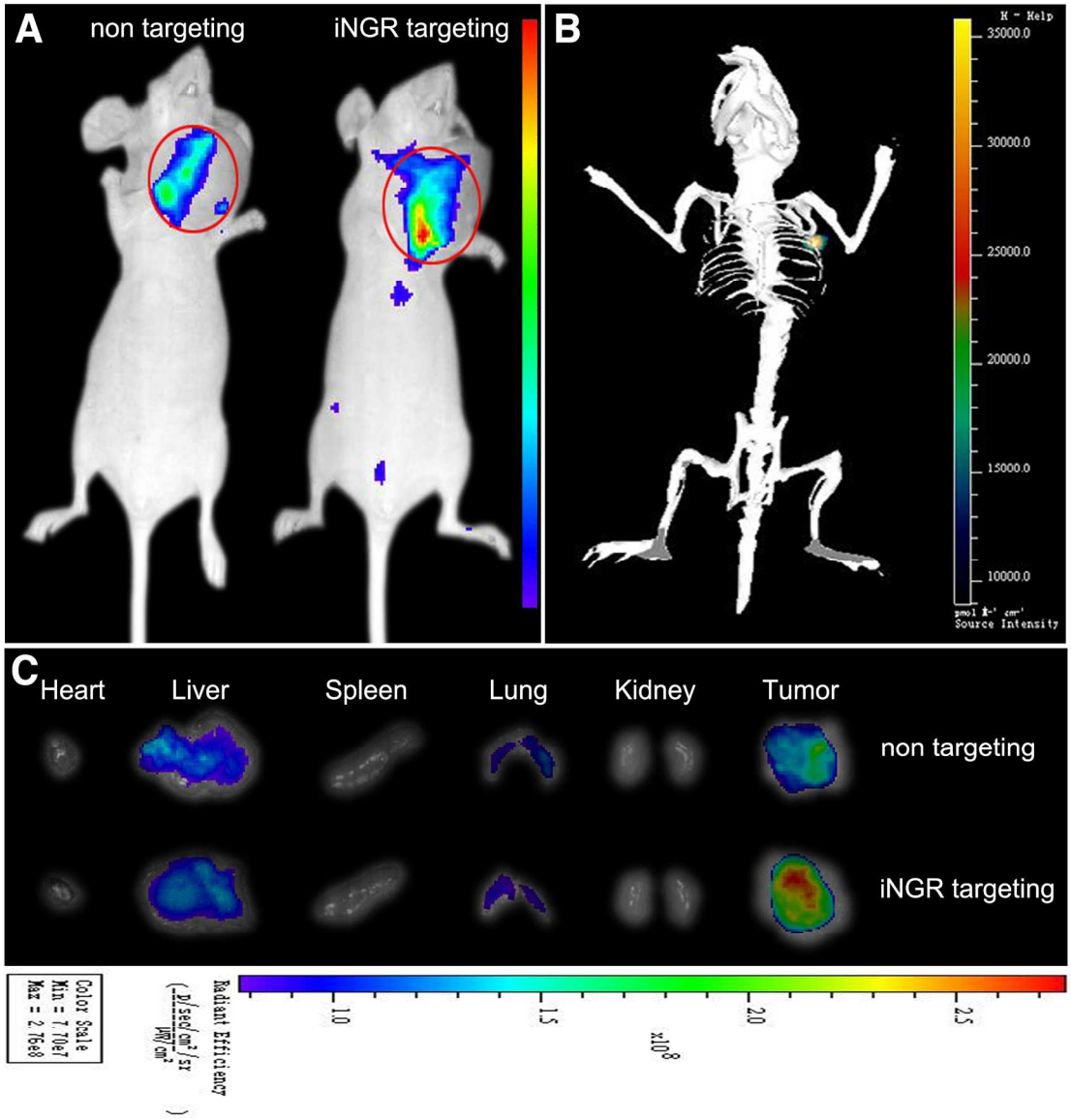

Figure 9. *In vivo* biodistribution and targeting effects of different PTX formulations in MDA-MB-231 bearing mice. (A) *In vivo* 2D imaging at 24 h after intravenous (iv) injection of MeO-PEG-PTX_8/PTX micelles (non targeting group) and iNGR-PEG-PTX_8/PTX micelles (iNGR targeting group) at a dose of 0.2 mg BODIPY/kg in tumor bearing mice (the red dotted circle was indicated as the location of tumor implantation); (B) *In vivo* 3D imaging at 24 h after i.v. injection of iNGR-PEG-PTX_8/PTX micelles in tumor-bearing mice; (C) Representative *ex vivo* optical images of tumors and organs of tumor-bearing mice sacrificed at 24 h.

Pharmacokinetics and biodistribution.

The mean plasma concentration-time profiles of PTX after intravenous administration of different PTX formulations were plotted in Figure 10, and the corresponding pharmacokinetic parameters were summarized in Table 4, respectively. As shown in Figure 10, the concentration of PTX in blood plasma decreased rapidly following the treatment of Taxol. Meanwhile, the concentration of PTX in blood plasma was maintained for a longer circulation time even after 24 h administration when treated with PTX micelles, due to the stable structure of the micelles. It was pretty clear that there were significant differences of the pharmacokinetic parameters between Taxol and the PEG-PTX_8/PTX micelles, where the mean area under the plasma-concentration curves ($AUC_{0-\infty}$) of MeO-PEG-PTX_8 micelles and iNGR-PEG_{5k}-PTX_8/PTX micelles were 6.52- and 5.81-fold higher than that of Taxol, respectively, corresponding mean residence time (MRT) of MeO-PEG-PTX_8/PTX micelle and iNGR-PEG-PTX_8/PTX micelle was 5.14- and 5.17-fold longer than that of Taxol, which suggest a prolonged blood circulation time of the polymeric micelles than Taxol. However, more studies are needed to fully understand the drug release and evaluate different fractions of the micelles in the plasma.

We next evaluated the *in vivo* biodistribution of PTX delivered to tumors by systemically injected MeO-PEG-PTX_8/PTX micelle, iNGR-PEG-PTX_8/PTX micelle and Taxol at the dose of 10 mg PTX/kg. Tissue samples of treated mice were collected by heart perfusion after 2 h and 24 h. Notably, the micelles significantly reduced the drug concentration at other organs, including heart, liver, spleen, lung and kidney at 2 h (Figure 11A). In particular, compared with Taxol, the level of PTX delivered by MeO-PEG-PTX_8/PTX micelles in the heart, liver, spleen, lung and kidney was lowered by 20.01-, 9.44-, 3.86-, 10.32- and 8.28-fold, respectively, and 16.45-, 3.62-, 6.68-, 6.88- and 17.41-fold, respectively by that of iNGR-PEG-PTX_8/PTX micelles.

Significantly, at 24 h after administration, iNGR-PEG-PTX_8/PTX and MeO-PEG-PTX_8/PTX micelles showed a 4.78- and 2.79-fold increase in drug concentration in the tumor, respectively, as compared with Taxol at the same dose (Figure 11B; two-way ANOVA; $P<0.001$). The decreased accumulation in the normal tissues is remarkable, as toxicity is the dose-dependent side effect of free PTX. Furthermore, the accumulation of PTX in the liver is also significantly lower for the mice treated with MeO-PEG-PTX_8/PTX micelles and iNGR-PEG-PTX_8/PTX micelles, compared with Taxol treatments. This is important because nanoparticles typically show significant accumulation in the liver while micelles with smaller size don't.

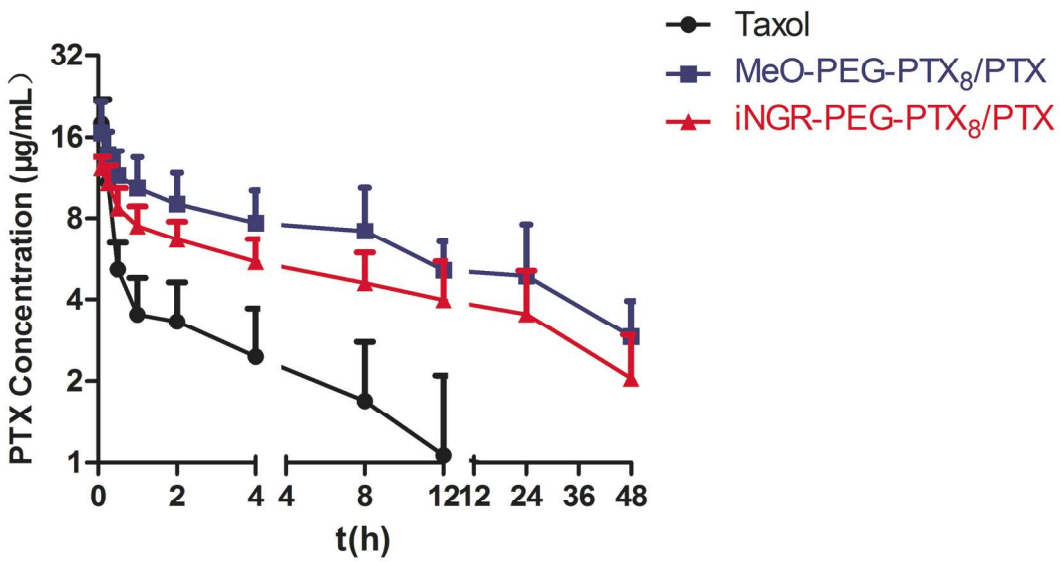

Figure 10. Pharmacokinetic profiles of PTX in SD rats after injection with different PTX formulations at a dose of 10 mg/kg. Data are represented as mean ± SD (n = 6).

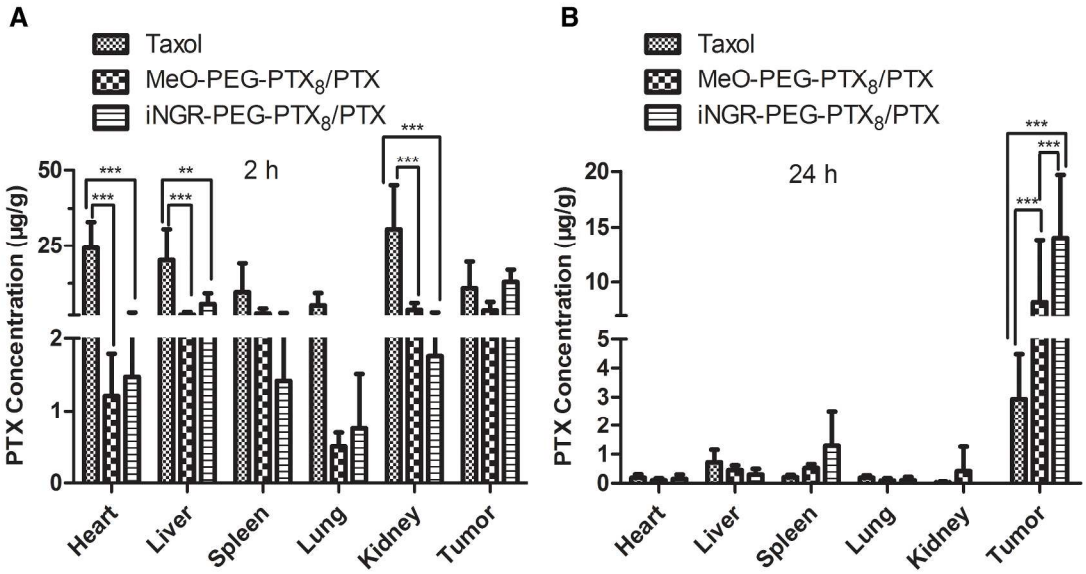

Figure 11. Concentration of PTX in tumor tissue and normal organs of MDA-MB-231 bearing nude mice at (A) 2 h and (B) 24 h after intravenous administration with Taxol, MeO-PEG-PTX_8/PTX and iNGR-PEG-PTX_8/PTX micelles at a dose of 10 mg/kg PTX. Data were presented as mean ± SD (n=4), **P < 0.01, ***P<0.001.

Table 4. Pharmacokinetic parameters of Taxol, MeO-PEG-PTX_8/PTX and iNGR-PEG-PTX_8/PTX micelles on SD rats (Data are presented as mean ± SD, n=6).

	Taxol	MeO-PEG-PTX_8/PTX	iNGR-PEG-PTX_8/PTX
AUC0-∞ (mg/L*h)	57.418 ± 38.685	374.463 ± 139.132	333.529 ± 178.994
MRT (h)	8.771 ± 3.761	45.115 ± 8.834	45.319 ± 21.562
Cl (L/h)	0.063 ± 0.038	0. 008 ± 0.004	0.008 ± 0.003
Vss (L)	0.442 ± 0.168	0.331 ± 0.125	0.342 ± 0.151
$t_{1/2}$ (h)	6.078 ± 2.606	31.264 ± 6.122	31.406 ± 14.942

Antitumor efficacy.

The antitumor efficacy was evaluated in TNBC-bearing mice after the treatment of different PTX formulations every four days for four times from day 15. Tumor volume and body weight of the nude mice were measured every other day. As shown in Figure 12A, compared with the control group, mice in all treatment groups exhibited a relatively slower growth rate of tumor volume and iNGR-PEG-PTX_8/PTX micelles displayed the strongest inhibition of tumor growth. Meanwhile, mice treated with PTX loaded micelles possessed a gentle change of body weight while the Taxol group demonstrated a decrease in body weight (Figure 12B).

The median survival time of the TNBC-bearing nude mice was also monitored. The survival time was significantly prolonged for iNGR-PEG-PTX_8/PTX treated group. To be specific, the median survival time was 43 days for iNGR-PEG-PTX_8/PTX treated group, 37.5 days for MeO-PEG-PTX_8/PTX micelle treated group, 34 days for Taxol treated group and 30 days for saline treated group (Figure 12C).

TUNEL assay was adopted to further detect the apoptosis of tumor cells. TNBC-bearing nude mice administrated with different PTX formulations were anaesthetized with 8% chloral hydrate in saline and tumors were excised followed by heart perfusion and fixation with 4% paraformaldehyde. Compared with the control group, Taxol and tumors treated with MeO-PEG-PTX_8/PTX micelle displayed weak green signal while iNGR-PEG-PTX_8/PTX demonstrated significantly enhanced green fluorescence that represents cell apoptosis (Figure 13). The results indicated that with iNGR peptide modification, the micelles showed enhanced tumor targeting and penetrating ability to induce more tumor cell apoptosis.

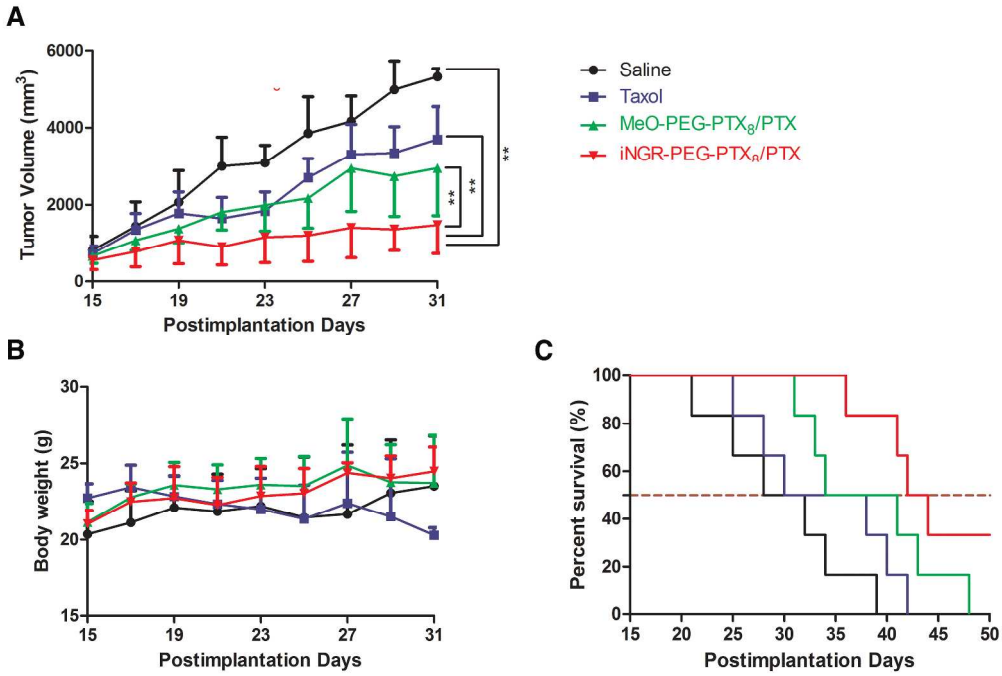

Figure 12. Evaluation of *in vivo* anti-tumor efficacy of different PTX formulations. (A) Tumor volume change, (B) body-weight change and (C) survival curve of MDA-MB-231 bearing mice after iv injections of Taxol, MeO-PEG-PTX_8/PTX and MeO-PEG-PTX_8/PTX micelles (10 mg/kg PTX) on days 15, 19, 23, and 27 (saline serving as control). Date are presented as mean ± SD (n = 6) (Two-way ANOVA, **P<0.01).

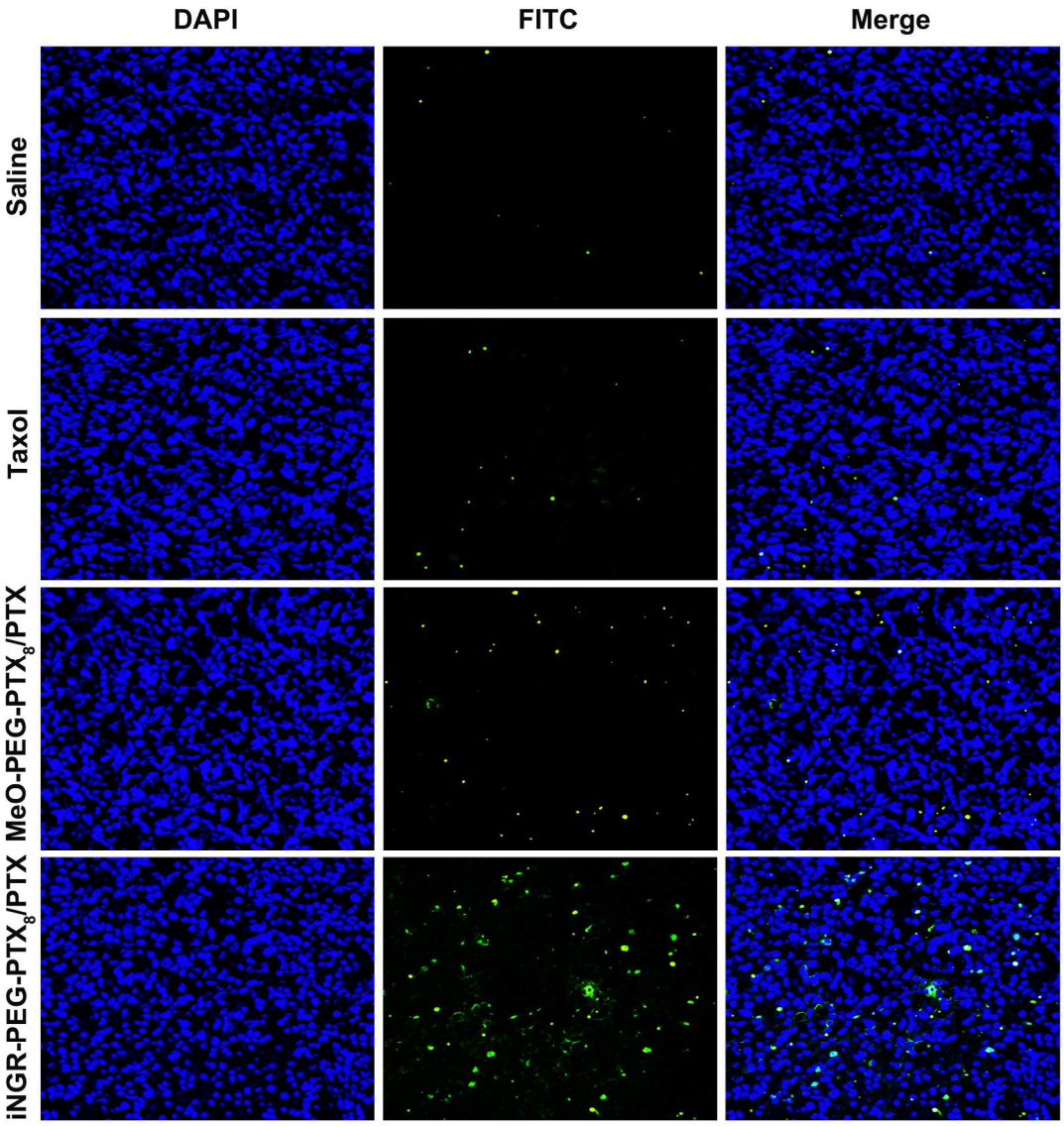

Figure 13. Representative histological images of MDA-MB-231 tumor xenografts excised from those nude mice used in the experiment of the *in vivo* antitumor efficacy of micelles. Blue: DAPI-stained cell nuclei; green: apoptosis cells (Original magnification: 100×).

Although the *in vitro* cytotoxicity results didn't show significant therapeutic benefit of the micelle groups (**Figure 7** and **Table 2**), the *in vivo* therapeutic effect of iNGR-PEG-PTX_8/PTX micelles was obviously better than Taxol. Taxol is hydrophilic and free PTX could passively diffuse into MDA-MB-231 cells, which is faster and easier than the internalization process of the

micelles, and the covalently linked PTX of the micelles was hydrolyzed insufficiently, so the intracellular prototype PTX concentration of Taxol group was higher than the micelle groups, while the intracellular PTX concentration iNGR-PEG-PTX_8/PTX micelle group is higher than MeO-PEG-PTX_8/PTX micelle group. As a result, the micelle groups showed higher IC_{50} value on MDA-MB-231 cells than Taxol group *in vitro*. However, the *in vitro* cytotoxicity assay didn't fully reflect the complicated conditions *in vivo*. Since the designed micelles have ultra-small size (~30 nm), they could passively target to tumor tissues (**Figure 9**) and accumulated more than Taxol (**Figure 11**) due to "EPR" effect, and thus the drug concentration in tumor tissue of the micelle groups is higher than Taxol, so the micelles could achieve better therapeutic effect. On the other hand, CD13 was overexpressed on tumor neovascular endothelial cells and NRP-1 was overexpressed on MDA-MB-231 breast cancer cells, and iNGR peptide exhibits tumor-homing and tumor-penetrating functions through the CD13 and NRP-1 receptors, so the iNGR-modified micelles displayed significantly enhanced targeting to TNBC (**Figure 9**) through CD13 and NRP-1 mediated pathway compared to MeO-PEG-PTX_8/PTX micelles. Therefore, PTX concentration of the iNGR-modified micelles in tumor tissue was higher than the non-targeting micelles (**Figure 11**), leading to better therapeutic effect.

Conclusion

In summary, we have successfully developed a novel linear-dendritic PEG-PTX_8 conjugate that can easily self-assembly into micelles with good morphology, ultra-small size and high drug loading capacity. The micelles showed high stability both *in vitro* and *in vivo*, which could maximize the EPR effect. Meanwhile, iNGR-PEG-PTX_8/PTX micelles showed higher cellular uptake and tumor accumulation by mediation of CD13 and NRP-1 receptors, lower drug concentration in normal tissues, and demonstrated strong anti-tumor effect for TNBC. Hopefully,

this novel linear-dendritic polymer drug conjugate may be a promising platform for targeted drug delivery in tumor therapy.

ASSOCIATED CONTENT

Supporting Information.

Characterization of the compounds during the synthetic process, stability studies of the MeO-PEG-PTX8/PTX and iNGR-PEG-PTX8/PTX micelles, cellular uptake studies on HUVECs and HEK293 cells treated with different modification percentage of iNGR peptide, the method, raw data and calculation of biodistribution assay (PDF).

AUTHOR INFORMATION

Corresponding Author

* Corresponding author: Chen Jiang, Tel: +86-21-5198-0079; Fax: +86-21-5198-0079; E-mail: jiangchen@shmu.edu.cn.

Present Addresses

Key Laboratory of Smart Drug Delivery, Ministry of Education, Department of Pharmaceutics. School of Pharmacy, Fudan University, 826 Zhangheng Road, Shanghai, 201203, China

Author Contributions

The manuscript was written through contributions of all authors. All authors have given approval to the final version of the manuscript.

Notes

The authors declare no competing financial interest.

ACKNOWLEDGMENT

This work was supported by the grants from National Basic Research Program of China (973 Program, grant no. 2013CB932500), National Science Fund for Distinguished Young Scholars (grant no. 81425023), and the National Natural Science Foundation of China (grant no. 81373355).

ABBREVIATIONS

NDDS: nano drug delivery system; PTX: paclitaxel; PDC: polymer-drug conjugate; EPR: enhanced permeation and retention; LDPDC: linear-dendritic polymer-drug conjugate; PEG: poly (ethylene glycol); TNBC: triple negative breast cancer; ER: estrogen receptor; PR: progesterone receptor; HER2: human epidermal growth factor receptor-2; HUVEC: Human umbilical vein endothelial cells; BBOPA: Benzylidene-2, 2-bis(oxymethyl) propionic anhydride; DCM: dichloromethane; CuAAC: copper(I)-catalyzed azide-alkyne cycloaddition; ACN: acetonitrile; NMR: nuclear magnetic resonance; HEPES: 4-(2-hydroxyethyl)-1-piperazineethanesulfonic acid; MTT: [4,5-dimethylthiazol-2-yl]-2,5-diphenyl tetrazolium bromide; TBME: tert-butyl methyl ether; TUNEL: terminal deoxynucleotidyl transferase dUTP nick-end labeling; MRT: mean residence time.

REFERENCES

(1) Chlebowski, R. T. Adriamycin (doxorubicin) cardiotoxicity: a review. *West J. Med*. **1979**, *131* (5), 364-368.

(2) Onetto, N.; Canetta, R.; Winograd, B.; Catane, R.; Dougan, M.; Grechko, J.; Burroughs, J.; Rozencweig, M. Overview of Taxol safety. *J. Natl. Cancer Inst. Monogr*. **1993**, 15, 131-139.

(3) Davis, M. E.; Chen, Z. G.; Shin, D. M. Nanoparticle therapeutics: an emerging treatment

modality for cancer. *Nat. Rev. Drug Discov*. **2008**, *7* (9), 771-782.

(4) Lv, S.; Tang, Z.; Zhang, D.; Song, W.; Li, M.; Lin, J.; Liu, H.; Chen, X. Well-defined polymer-drug conjugate engineered with redox and pH-sensitive release mechanism for efficient delivery of paclitaxel. *J. Control. Release*. **2014**, *194*, 220-227.

(5) Yoo, J. W.; Irvine, D. J.; Discher, D. E.; Mitragotri, S. Bio-inspired, bioengineered and biomimetic drug delivery carriers. *Nat. Rev. Drug Discov*. **2011**, *10* (7), 521-535.

(6) Tiwari, G.; Tiwari, R.; Sriwastawa, B.; Bhati, L.; Pandey, S.; Pandey, P.; Bannerjee, S. K. Drug delivery systems: An updated review. *Int. J. Pharm. Investig*. **2012**, *2* (1), 2-11.

(7) Liang, L.; Lin, S. W.; Dai, W.; Lu, J. K.; Yang, T. Y.; Xiang, Y.; Zhang, Y.; Li, R. T.; Zhang, Q. Novel cathepsin B-sensitive paclitaxel conjugate: Higher water solubility, better efficacy and lower toxicity. *J. Control. Release*. **2012**, *160* (3), 618-629.

(8) Iyer, A. K.; Khaled, G.; Fang, J.; Maeda, H. Exploiting the enhanced permeability and retention effect for tumor targeting. *Drug Discov. Today*. **2006**, *11* (17-18), 812-818.

(9) Dawidczyk, C. M.; Kim, C.; Park, J. H.; Russell, L. M.; Lee, K. H.; Pomper, M. G.; Searson, P. C. State-of-the-art in design rules for drug delivery platforms: lessons learned from FDA-approved nanomedicines. *J. Control. Release*. **2014**, *187*, 133-144.

(10) Bozzuto, G.; Molinari, A. Liposomes as nanomedical devices. *Int. J. Nanomedicine*. **2015**, *10*, 975-999.

(11) Ferrari, M. Cancer nanotechnology: opportunities and challenges. *Nat. Rev. Cancer*. **2005**, *5* (3), 161-171.

(12) Geng, Y.; Discher, D. E. Visualization of degradable worm micelle breakdown in relation to drug release. *Polymer*. **2006**, *47* (7), 2519-2525.

(13) Li, C.; Li, Y.; Gao, Y.; Wei, N.; Zhao, X.; Wang, C.; Li, Y.; Xiu, X.; Cui, J. Direct

comparison of two albumin-based paclitaxel-loaded nanoparticle formulations: is the crosslinked version more advantageous? *Int. J. Pharm*. **2014**, *468* (1-2), 15-25.

(14) Zhao, M.; Lei, C.; Yang, Y.; Bu, X.; Ma, H.; Gong, H.; Liu, J.; Fang, X.; Hu, Z.; Fang, Q. Abraxane, the Nanoparticle Formulation of Paclitaxel Can Induce Drug Resistance by Up-Regulation of P-gp. *PLoS One*. **2015**, *10* (7), e0131429.

(15) Khandare, J.; Minko, T. Polymer–drug conjugates: Progress in polymeric prodrugs. *Progress in Polymer Science*. **2006**, *31* (4), 359-397.

(16) Kopecek, J. Polymer-drug conjugates: origins, progress to date and future directions. *Adv. Drug Deliv. Rev*. **2013**, *65* (1), 49-59.

(17) Hu, X.; Jing, X. Biodegradable amphiphilic polymer-drug conjugate micelles. *Expert Opin. Drug Deliv*. **2009**, *6* (10), 1079-1090.

(18) Gao, G. H.; Li, Y.; Lee, D. S. Environmental pH-sensitive polymeric micelles for cancer diagnosis and targeted therapy. *J. Control. Release*. **2013**, *169* (3), 180-184.

(19) Tam, Y. T.; Gao, J.; Kwon, G. S. Oligo(lactic acid)n-Paclitaxel Prodrugs for Poly(ethylene glycol)-block-poly(lactic acid) Micelles: Loading, Release, and Backbiting Conversion for Anticancer Activity. *J. Am. Chem. Soc*. **2016**, *138* (28), 8674-8677.

(20) Wang, J.; Mao, W.; Lock, L. L.; Tang, J.; Sui, M.; Sun, W.; Cui, H.; Xu, D.; Shen, Y. The Role of Micelle Size in Tumor Accumulation, Penetration, and Treatment. *ACS Nano*. **2015**, *9* (7), 7195-7206.

(21) Chuan, X.; Song, Q.; Lin, J.; Chen, X.; Zhang, H.; Dai, W.; He, B.; Wang, X.; Zhang, Q. Novel free-paclitaxel-loaded redox-responsive nanoparticles based on a disulfide-linked poly(ethylene glycol)-drug conjugate for intracellular drug delivery: synthesis, characterization, and antitumor activity in vitro and in vivo. *Mol. Pharm*. **2014**, *11* (10), 3656-3670.

(22) Zhou, Z.; Ma, X.; Jin, E.; Tang, J.; Sui, M.; Shen, Y.; Van Kirk, E. A.; Murdoch, W. J.; Radosz, M. Linear-dendritic drug conjugates forming long-circulating nanorods for cancer-drug delivery. *Biomaterials*. **2013**, *34* (22), 5722-5735.

(23) Li, C.; Wallace, S. Polymer-drug conjugates: recent development in clinical oncology. *Adv. Drug Deliv. Rev*. **2008**, *60* (8), 886-898.

(24) Zhang, Y.; Chan, H. F.; Leong, K. W. Advanced materials and processing for drug delivery: the past and the future. *Adv. Drug Deliv. Rev*. **2013**, *65* (1), 104-120.

(25) Yokoyama, M. Polymeric micelles as drug carriers: their lights and shadows. *J. Drug Target*. **2014**, *22* (7), 576-583.

(26) Xiao, W.; Luo, J.; Jain, T.; Riggs, J. W.; Tseng, H. P.; Henderson, P. T.; Cherry, S. R.; Rowland, D.; Lam, K. S. Biodistribution and pharmacokinetics of a telodendrimer micellar paclitaxel nanoformulation in a mouse xenograft model of ovarian cancer. *Int. J. Nanomedicine*. **2012**, *7*, 1587-1597.

(27) Lee, C. C.; MacKay, J. A.; Frechet, J. M.; Szoka, F. C. Designing dendrimers for biological applications. *Nat. Biotechnol*. **2005**, *23* (12), 1517-1526.

(28) Wei, T.; Chen, C.; Liu, J.; Liu, C.; Posocco, P.; Liu, X.; Cheng, Q.; Huo, S.; Liang, Z.; Fermeglia, M.; Pricl, S. Anticancer drug nanomicelles formed by self-assembling amphiphilic dendrimer to combat cancer drug resistance. *Proc. Natl. Acad. Sci. U S A*. **2015**, *112* (10), 2978-2983.

(29) Li, J.; Yang, H.; Zhang, Y.; Jiang, X.; Guo, Y.; An, S.; Ma, H.; He, X.; Jiang, C. Choline Derivate-Modified Doxorubicin Loaded Micelle for Glioma Therapy. *ACS Appl. Mater. Interfaces*. **2015**, *7* (38), 21589-21601.

(30) Harris, J. M.; Chess, R. B. Effect of pegylation on pharmaceuticals. *Nat. Rev. Drug Discov*.

2003, *2* (3), 214-221.

(31) Pasut, G.; Veronese, F. M. PEG conjugates in clinical development or use as anticancer agents: an overview. *Adv. Drug Deliv. Rev*. **2009**, *61* (13), 1177-1188.

(32) Pasqualini, R.; Koivunen, E.; Kain, R.; Lahdenranta, J.; Sakamoto, M.; Stryhn, A.; Ashmun, R. A.; Shapiro, L. H.; Arap, W.; Ruoslahti, E. Aminopeptidase N is a receptor for tumor-homing peptides and a target for inhibiting angiogenesis. *Cancer Res*. **2000**, *60* (3), 722-727.

(33) Jubb, A. M.; Strickland, L. A.; Liu, S. D.; Mak, J.; Schmidt, M.; Koeppen, H. Neuropilin-1 expression in cancer and development. *J. Pathol*. **2012**, *226* (1), 50-60.

(34) Slimani, H.; Guenin, E.; Briane, D.; Coudert, R.; Charnaux, N.; Starzec, A.; Vassy, R.; Lecouvey, M.; Perret, Y. G.; Cao, A. Lipopeptide-based liposomes for DNA delivery into cells expressing neuropilin-1. *J. Drug Target*. **2006**, *14* (10), 694-706.

(35) Feng, G. K.; Liu, R. B.; Zhang, M. Q.; Ye, X. X.; Zhong, Q.; Xia, Y. F.; Li, M. Z.; Wang, J.; Song, E. W.; Zhang, X.; Wu, Z. Z.; Zeng, M. S. SPECT and near-infrared fluorescence imaging of breast cancer with a neuropilin-1-targeting peptide. *J. Control Release*. **2014**, *192*, 236-242.

(36) Alberici, L.; Roth, L.; Sugahara, K. N.; Agemy, L.; Kotamraju, V. R.; Teesalu, T.; Bordignon, C.; Traversari, C.; Rizzardi, G. P.; Ruoslahti, E. De novo design of a tumor-penetrating peptide. *Cancer Res*. **2013**, *73* (2), 804-812.

(37) Curnis, F.; Arrigoni, G.; Sacchi, A.; Fischetti, L.; Arap, W.; Pasqualini, R.; Corti, A. Differential binding of drugs containing the NGR motif to CD13 isoforms in tumor vessels, epithelia, and myeloid cells. *Cancer Res*. **2002**, *62* (3), 867-874.

(38) Hou, L.; Yao, J.; Zhou, J. Simultaneous LC–MS Analysis of Paclitaxel and Retinoic Acid in Plasma and Tissues from Tumor-Bearing Mice. *Chromatographia*. **2011**, *73* (5), 471-480.

(39) Kim, S. H.; Tan, J. P.; Fukushima, K.; Nederberg, F.; Yang, Y. Y.; Waymouth, R. M.;

Hedrick, J. L. Thermoresponsive nanostructured polycarbonate block copolymers as biodegradable therapeutic delivery carriers. *Biomaterials*. **2011**, *32* (23), 5505-5514.

(40) Chen, W.; Meng, F.; Cheng, R.; Deng, C.; Feijen, J.; Zhong, Z. Advanced drug and gene delivery systems based on functional biodegradable polycarbonates and copolymers. *J. Control. Release*. **2014**, *190*, 398-414.

(41) Cordes, N.; Plasswilm, L. Cell line and schedule-dependent cytotoxicity of paclitaxel (Taxol): role of the solvent Cremophor EL/ethanol. *Anticancer Res*. **1998**, *18* (3a), 1851-1857.

(42) Plasswilm, L.; Cordes, N.; Fietkau, R.; Sauer, R. Cytotoxicity of fractionated paclitaxel (Taxol) administration in vitro. *Strahlenther. Onkol*. **1998**, *174* (1), 37-42.

(43) Fjallskog, M. L.; Frii, L.; Bergh, J. Is Cremophor EL, solvent for paclitaxel, cytotoxic? *Lancet*. **1993**, *342* (8875), 873.

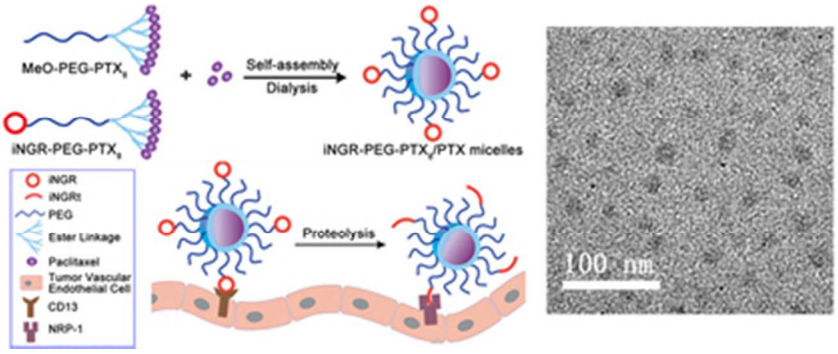

Table of Contents/Abstract Graphic

35x14mm (300 x 300 DPI)